Electronic Supplementary Information

Gauging surface charge distribution of live cell membrane by ionic current change using scanning ion conductance microscopy

Feng Chen[a, b], Jin He[*b], Prakash Manandhar[c], Yizi Yang[a], Peidang Liu[d], Ning Gu [*a, d]
[a]School of biomedical engineering and informatics, Nanjing Medical University, Nanjing 211166, People's Republic of China
[b]Physics Department, Biomolecular Science Institute, Florida International University, Miami, FL 33199, United States
[c]Department of chemistry and biochemistry, Florida International University, Miami, FL 33199, United States
[d]Jiangsu Key Laboratory for Biomaterials and Devices, School of Biological Science and Medical Engineering, Southeast University, Nanjing 210009, China

ESI-1. Nanopipette characterization

The pore geometry of nanopipette is mainly defined by the half cone angle and pore diameter. The nanopipette was filled with the same electrolyte as the bath solution and an Ag/AgCl wire electrode was inserted from the back. The current-voltage curves (IV) of the nanopipette were measured by a source measure unit 2636A (Keithley Instruments, Cleveland, Ohio). Electric bias was applied below 0.5 V, generally (-0.4 to +0.4 V) with a scan rate of 50 mV/s to avoid hydrolysis and instability of reference electrodes. The pore diameter D can be calculated by a simple equation:

$$D = \frac{2}{kR_p}\left(\frac{1}{\pi tan\theta}\right) \quad \text{S1}$$

where k is the conductivity of 1×PBS buffer and R_p is the pore resistance determined by the slope of the linear IV curve within a bias range between -35 mV and 35 mV. From the pore resistance 0.168 GΩ and half cone angle 2, the calculated pore diameter D is about 70 nm. The calculated size is consistent with the SEM image. More details of the fitting and pore size calculation can be found in previous paper.[1]

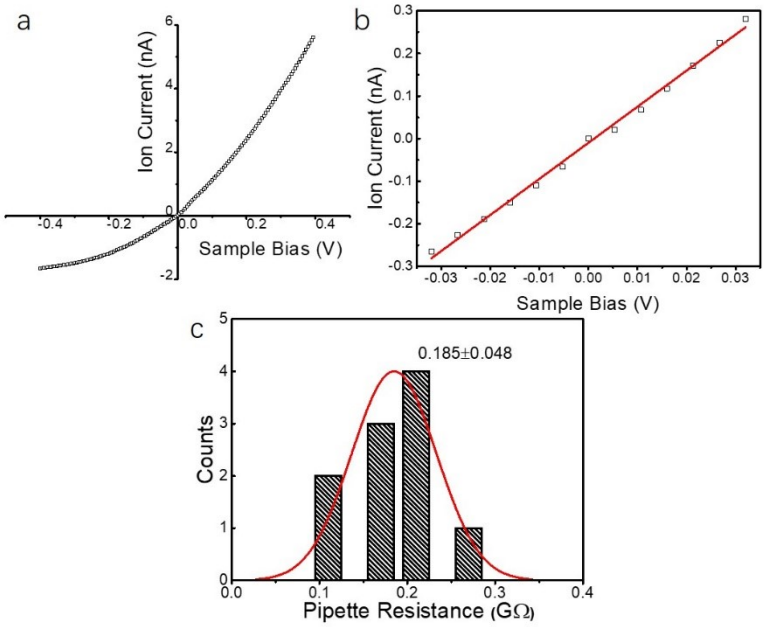

Figure S1. (a) The IV curve of a typical borosilicate glass nanopipette in 1×PBS before approaching to the substrate. **(b)** The IV curve at a small applied bias range (-30.5 mV to +30.5 mV). The red curve is the linear fitting to the experimental data, and the pore resistance R_{pore}=0.168 GΩ was obtained from the slope of the fitting line. **(c)** The histogram of the R_p of 10 nanopipettes. The red curve is the Gaussian fit, and the mean value is 0.185 ± 0.048 GΩ.

ESI-2. Surface modification of PDMS and Au/PDMS substrates

PDMS substates were prepared by mixing 1 part of curing agent with 10 parts of silicone elastomer base (SYLGARD, Dow Corning, USA) in plastic petri dishes, and then degassed in a vacuum oven for 30 min and cured at room temperature for two days. The top surface of the PDMS substrate in the petri dish was used for imaging. The modification of PDMS can be seen as previously described.[2] Briefly, the PDMS substrates were subjected to oxygen plasma for 5 min in a plasma cleaner (Harrick Plasma-PDC 001), followed by immersed in 5% 3-aminopropyltriethoxysilane (APTES) solution for 1 h. The APTES modified PDMS substrates were further immersed in 0.5% glutaraldehyde solution for 1 h and 5% bovine serum albumin (BSA) solution for 3h, rinsed with deionized

water, and then dried in Ar flow. The schematic diagram and approach curves on both the APTES and BSA modified PDMS substrates in 1×PBS buffer are shown in Figure S2.

To prepare gold coated PDMS substrates, the PDMS substrates were immersed in a mixture solution containing $HAuCl_4$ (20 mM), $KHCO_3$ (0.5 M), and glucose (25 mM) at 45 °C until a visible golden color layer was formed.[3] Then the gold decorated PDMS substrates were immersed in 1 mM 4-MBA or 4-ATP ethanol solution overnight. The schematic diagrams of PDMS modification are shown in Figures S3a. The SEM images of the formed gold layer in Figure S3b further illustrate the roughness of the surface.[4] We then modified 4-MBA and 4-ATP on the gold layers, as proved by Raman spectroscopy in Figure S3c. For modified Au/PDMS substrates, the two main peaks at 1085 cm^{-1} and 1590 cm^{-1} appeared, which attributed to the stretching of C-S bond and the C-C bond on the benzene ring. We confirmed that the b_2-type bands (1147 cm^{-1}, 1398 cm^{-1}) and the a_1-type bands (1581 cm^{-1}) appeared on 4-ATP-Au/PDMS substrate (Figure 3c(i)). And the bands around 1410 cm^{-1} ($-COO^-$), 1710 cm^{-1} (-C=O), and 1590 cm^{-1} (C-C) appeared on 4-MBA-Au/PDMS substrate, as shown in Figure 3c(ii).

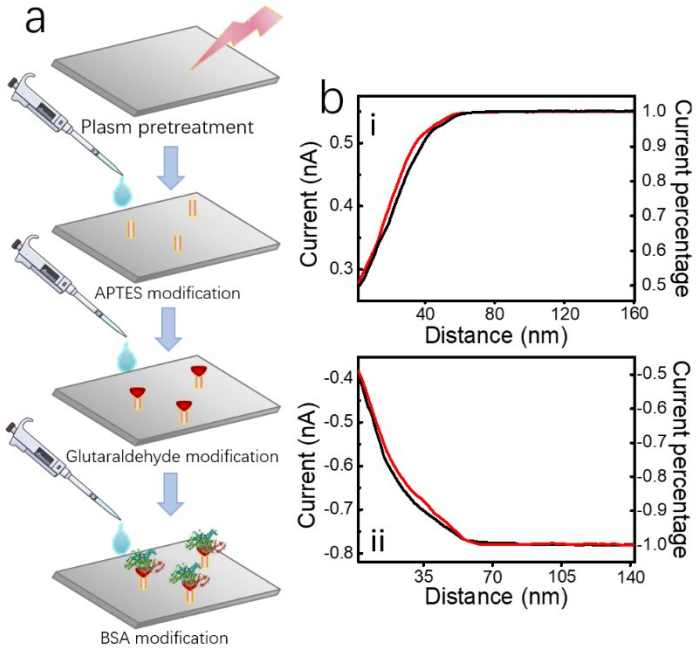

Figure S2. (a) Schematic diagram of surface modification of PDMS substrates. **(b)** Approach curves for ionic current on APTES-PDMS (black) and BSA-PDMS (red) using +0.1 V V_t (i) and -0.1 V V_t (ii).

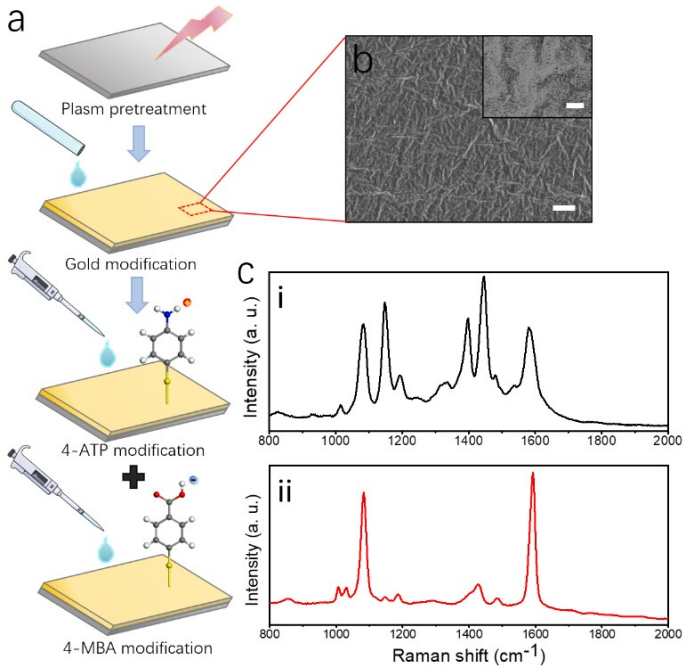

Figure S3. (a) Schematic diagram of the procedures for surface modification of Au/PDMS substrates. **(b)** SEM images of Au/PDMS substrates (scale bar: 10 µm; inset scale bar: 1 µm). **(c)** SERS spectra of 4-ATP (i) and 4-MBA (ii) modified Au/PDMS substrates using 632.8 nm radiation as the excitation source.

ESI-3. Time traces acquired during coarse scan and fine scan

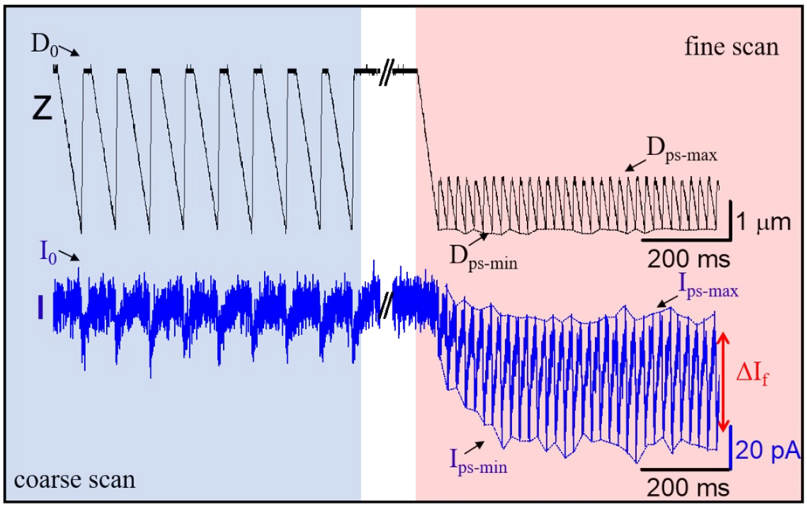

Figure S4. The time traces of nanopipette displacement (Z) and current (I) during the coarse and fine scan over BSA-PDMS substrate using +0.1 V V_s.

ESI-4. FEM simulations

All FEM computations were performed using COMSOL Multiphysics (5.4) with AC/DC and chemical reaction engineering modules. To simplify the computations, the system was assumed at a steady state, and the fluidic flow term was not included. A 2D axisymmetric model used for FEM simulations is depicted in Figure S5. The nanopore diameter was set to 70 nm, the nanopipette walls were fixed at 15 nm thick, and the D_{ps} was varied. The whole computation domain was discretized into free triangular elements, and the mesh size was 11.1 nm. To simplify the simulations, only two ions, potassium and chlorine, were used at 150 M concentration. The electric potential distribution was modelled by the Poisson equation:

$$\nabla^2 \emptyset = -\frac{F}{\epsilon}\sum_i z_i c_i$$

where $\emptyset$ is the local electric potential, F is the Faraday's constant, ϵ is a dielectric constant in electrolyte solution, z_i is the charge of species I, and ci is the concentration. The ion transport was described by the Nernst-Plank equation:

$$J_i = -D_i \nabla c_i - \frac{z_i F}{TR} D_i C_i \nabla \emptyset$$

in above equation, J_i is the ion flux vector, D_i is the diffusion coefficient, T is the temperature and R is the gas constant. The steady-state current and electric potential were simulated subject to the following boundary conditions and related physics equations shown in Table S1.

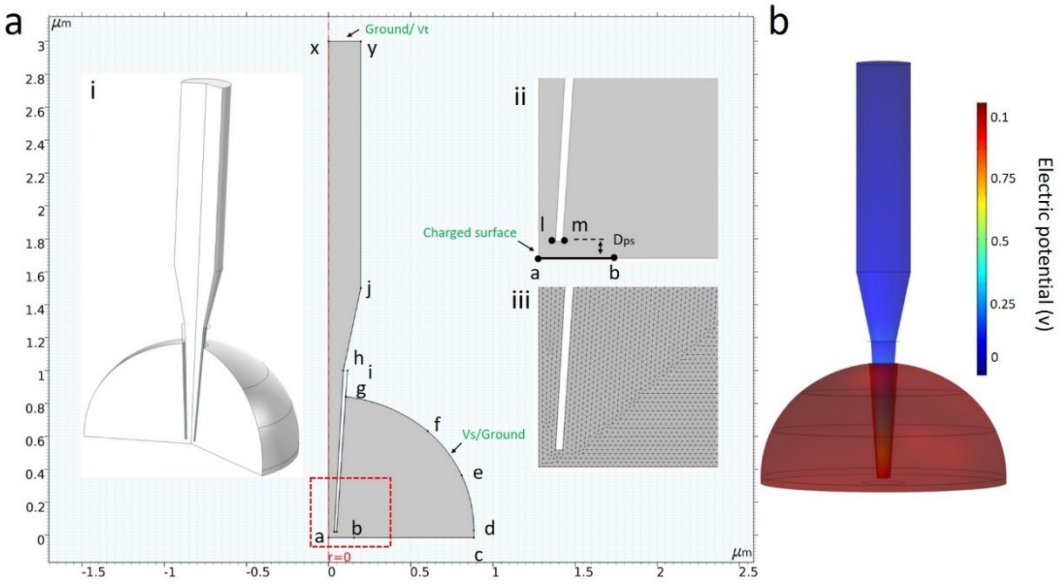

Figure S5. (a) 2D axial symmetric geometry of the nanopipette used for the FEM simulations (r=0 indicates the axis symmetry line). Insets: **(i)** the 3D view of the simulation model. **(ii)** zoom-in view of the tip region with a hemispherical shape with radius of 35 nm. **(iii)** mesh distribution near the tip of hemispherical shape. **(b)** Electric potential distribution near the tip region on a negatively charged surface (-25 mC/m^2) using +0.1 V V_s.

Table S1: Boundary conditions and related physics equations.

Surface	Poisson's Equation	Nernst-Plank Equation
ax	Axial symmetry	Axial symmetry
ab	Substrate with surface charge (±25 mC/m^2)	No flux (insulation)
bc/cd/de/fg/hj/jy	Zero charge	No flux (insulation)
lh/lm/mg (quartz)	-5 mC/m^2	No flux (insulation)
ef/xy	Ground/ Potential applied (±0.1 V)	Constant concentration

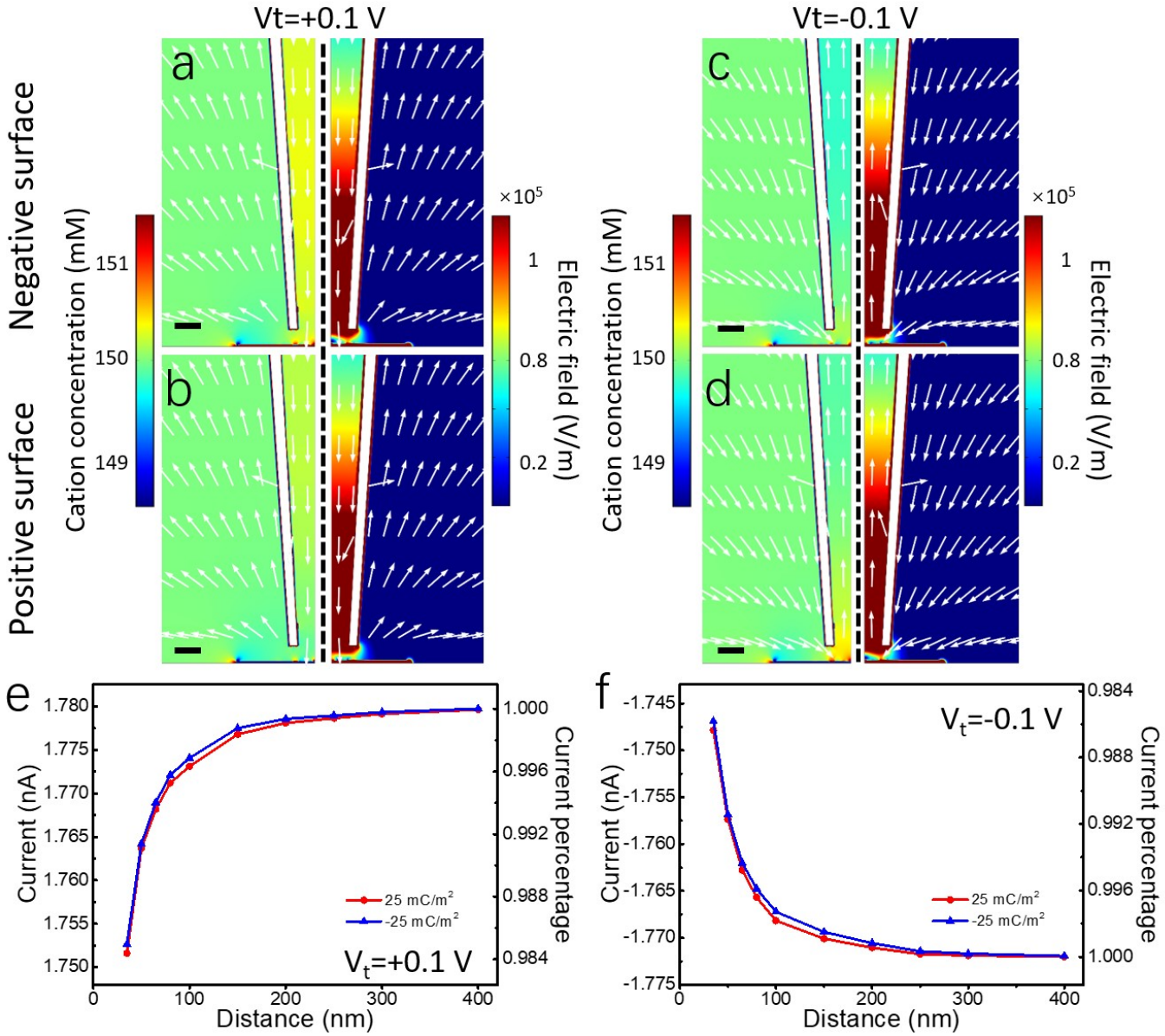

Figure S6. (a-d) FEM simulation results of cation concentration (on the left of each subsection) and electric field distribution (on the right of each subsection) near the tip of negatively charged nanopipette over different charged substrates using V_t biases (scale bar: 50 nm). Data are obtained from a negatively charged surface (-25 mC/m^2) at D_{ps}=35 nm using +0.1 V V_t **(a)** and -0.1 V V_t **(c)**; a

positively charged surface (25 mC/m^2) at D_{ps}=35 nm using +0.1 V V_t **(b)** and -0.1 V V_t **(d)**. The mass-transport of the cations and the direction of the electric field are denoted with white arrows. **(e-f)** The simulated current changes versus D_{ps} using V_t=+0.1 V **(e)** and V_t=-0.1 V **(f)**.

ESI-5. The ionic current traces before and after imaging

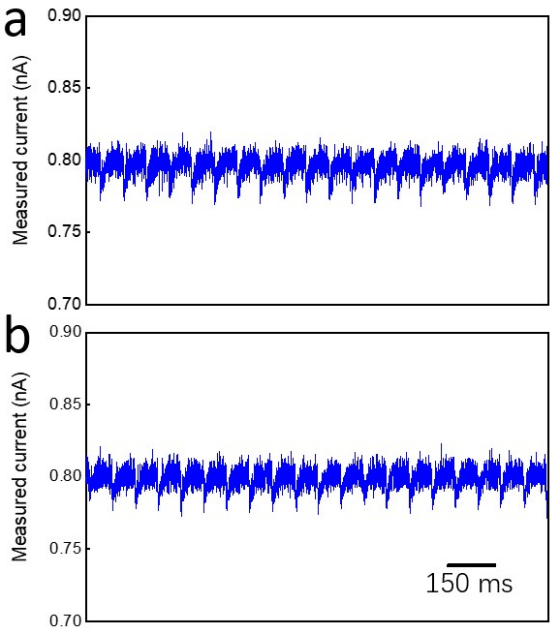

Figure S7. The ionic current traces of coarse scan before **(a)** and after **(b)** the imaging of a BSA-PDMS substrate using +0.1 V V_s.

ESI-6. Surface charge contrast mapping of flat PDMS substrates

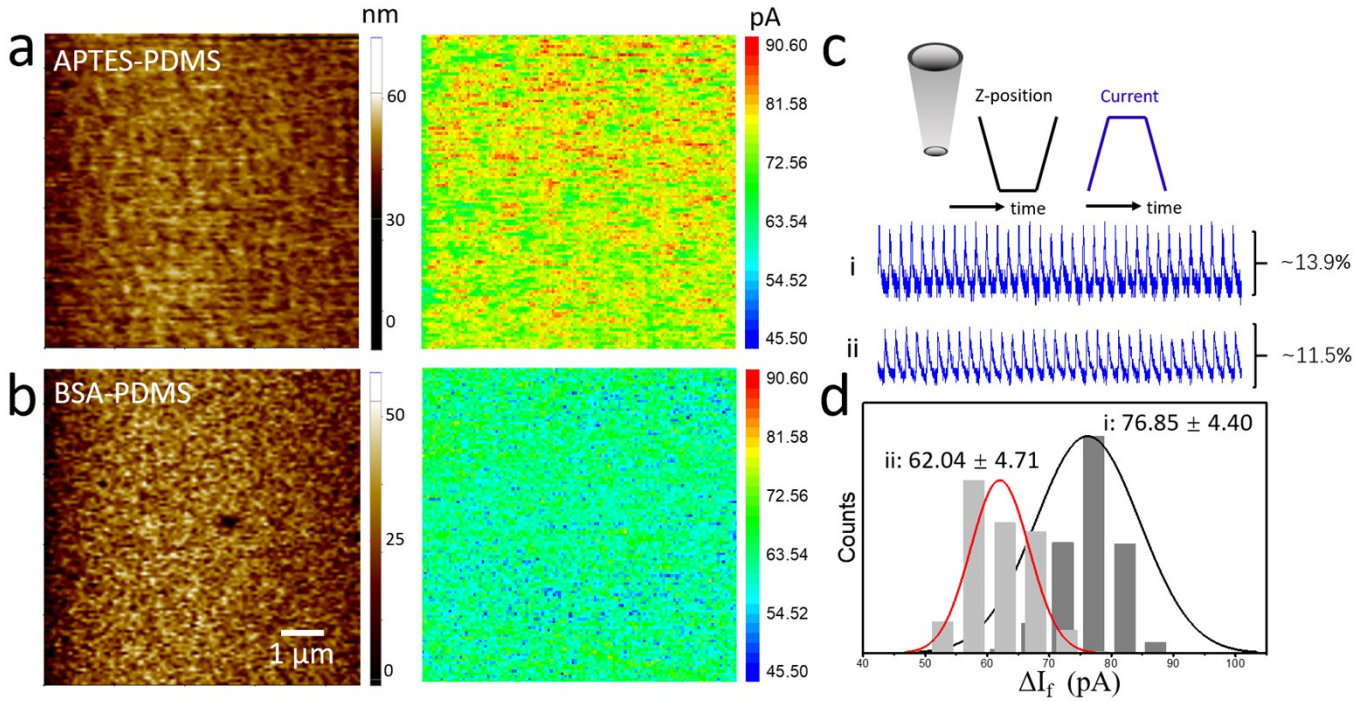

Figure S8. (a-b) The representative topography (left) and surface charge (ΔI_f) contrast images (right) of PDMS substrates modified with APTES **(a, positively charged)** and BSA **(b, negatively charged)** using -0.1 V V_s. **(c-d)** The typical I_f time traces **(c)** and the ΔI_f histograms **(d)** on APTES-PDMS (i) and BSA-PDMS (ii) substrates. All images were recorded in 1×PBS buffer.

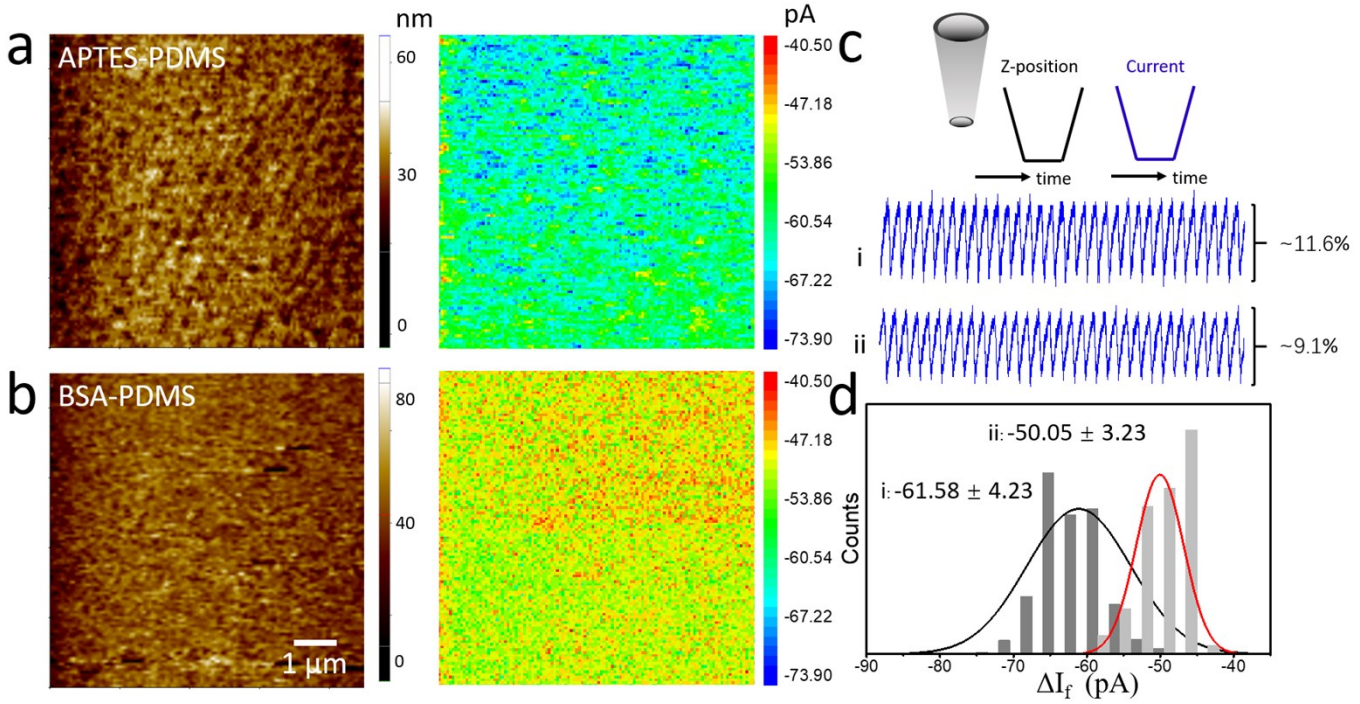

Figure S9. (a-b) The representative topography (left) and surface charge (ΔI_f) contrast images (right) of PDMS substrates modified with APTES **(a, positively charged)** and BSA **(b, negatively charged)** using +0.1 V V_t. **(c-d)** The typical I_f time traces **(c)** and the ΔI_f histograms **(d)** on APTES-PDMS (i) and BSA-PDMS (ii) substrates.

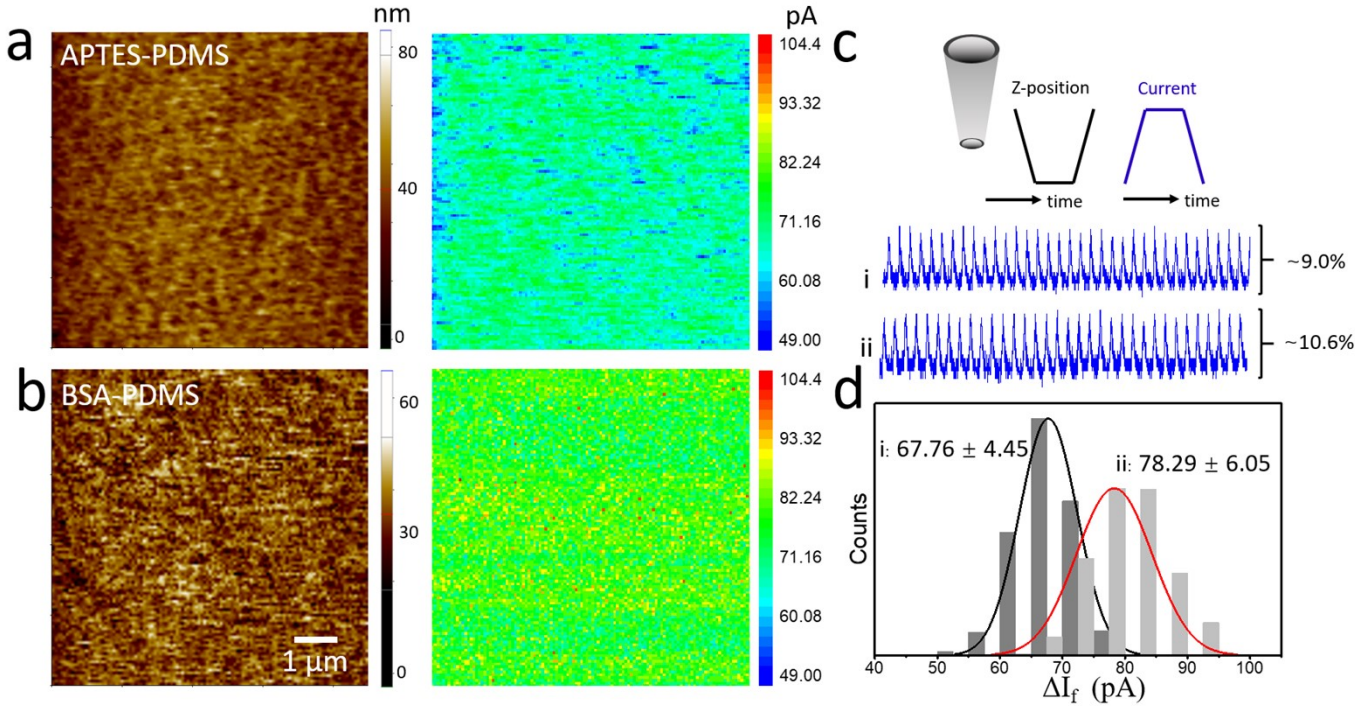

Figure S10. (a-b) The representative topography (left) and surface charge (ΔI_f) contrast images (right) of PDMS substrates modified with APTES **(a, positively charged)** and BSA **(b, negatively charged)** using -0.1 V V_t. **(c-d)** The typical I_f time traces **(c)** and the ΔI_f histograms **(d)** on APTES-PDMS (i) and BSA-PDMS (ii) substrates.

ESI-7. Surface charge contrast mapping of rough Au/PDMS substrates

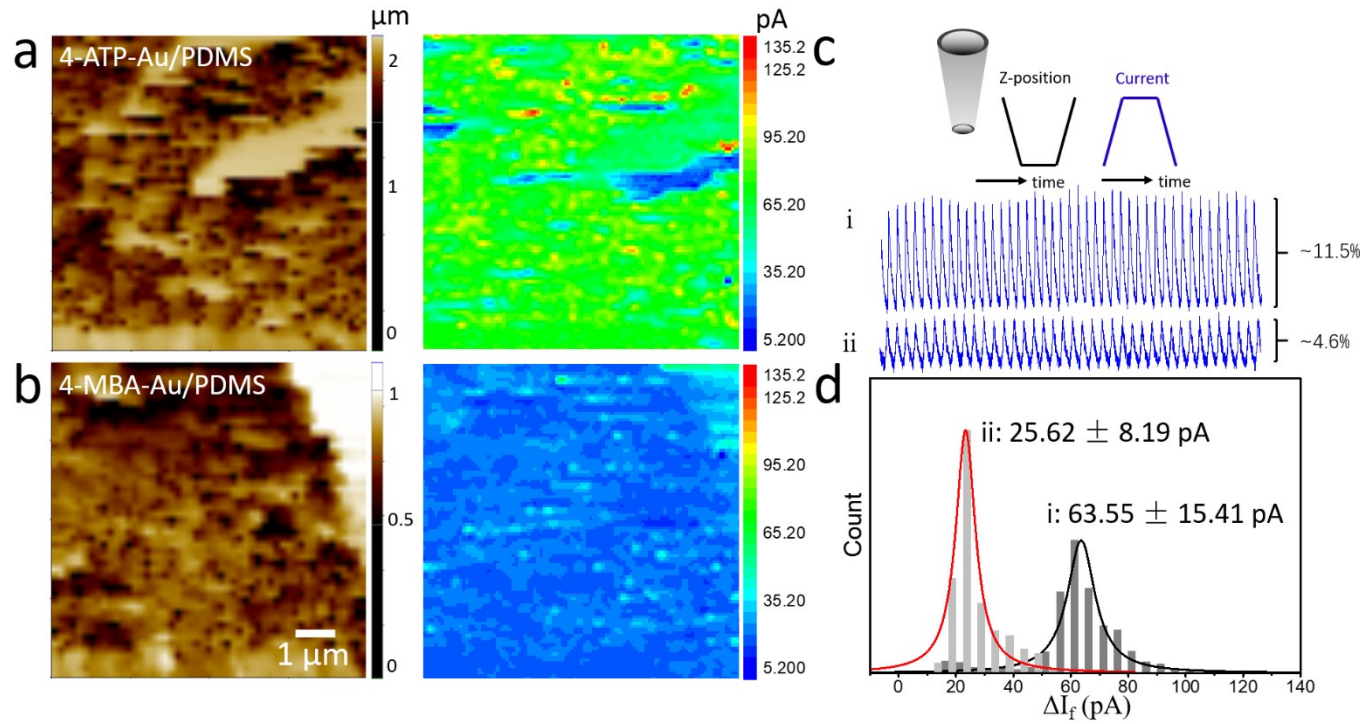

Figure S11. (a-b) The representative topography (left) and surface charge (ΔI_f) contrast images (right) of Au/PDMS substrates modified with 4-ATP **(a, positively charged)** and 4-MBA **(b, negatively charged)** using -0.1 V V_s. **(c-d)** The typical I_f time traces (c) and the ΔI_f histograms (d) on 4-ATP-Au/PDMS (i) and 4-MBA-Au/PDMS (ii) substrates. All images were recorded in 1×PBS buffer.

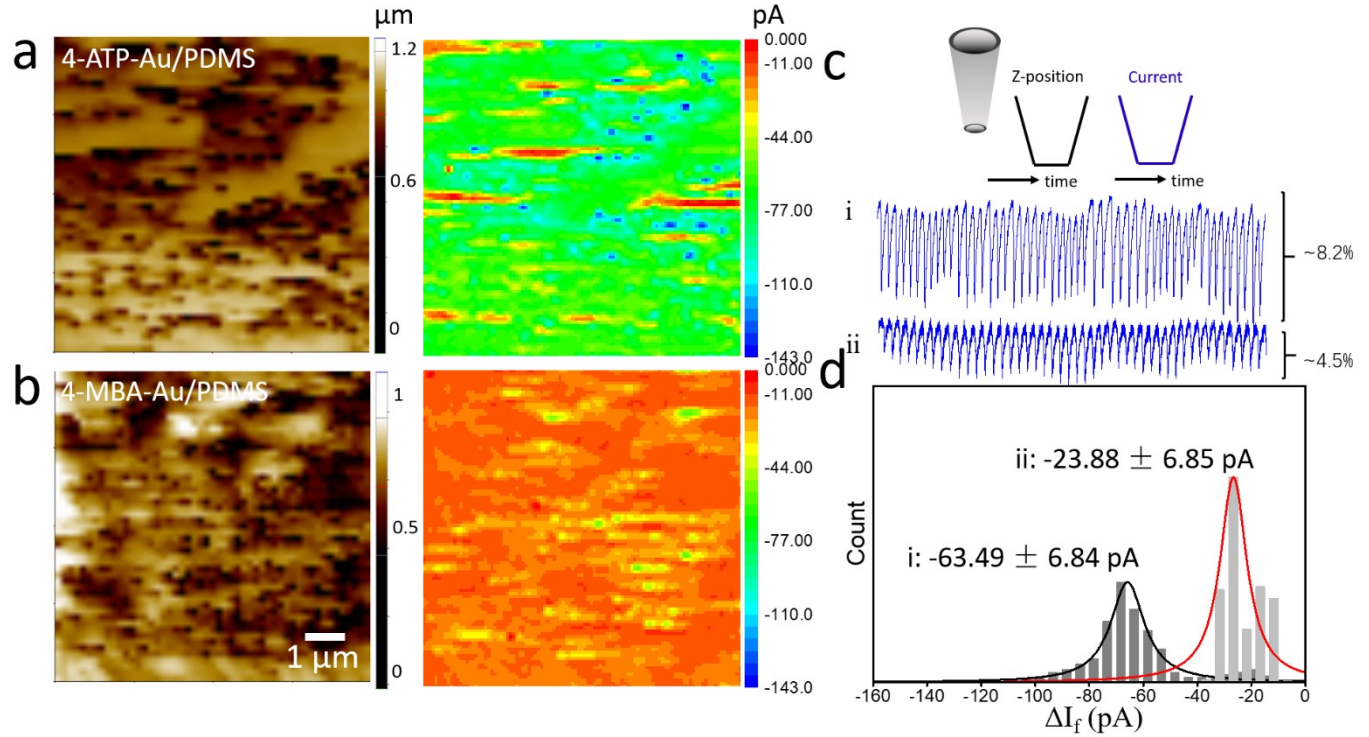

Figure S12. (a-b) The representative topography (left) and surface charge (ΔI_f) contrast images (right) of Au/PDMS substrates modified with 4-ATP **(a, positively charged)** and 4-MBA **(b, negatively charged)** using +0.1 V V_t. **(c-d)** The typical I_f time traces **(c)** and the ΔI_f histograms **(d)** on 4-ATP-Au/PDMS (i) and 4-MBA-Au/PDMS (ii) substrates.

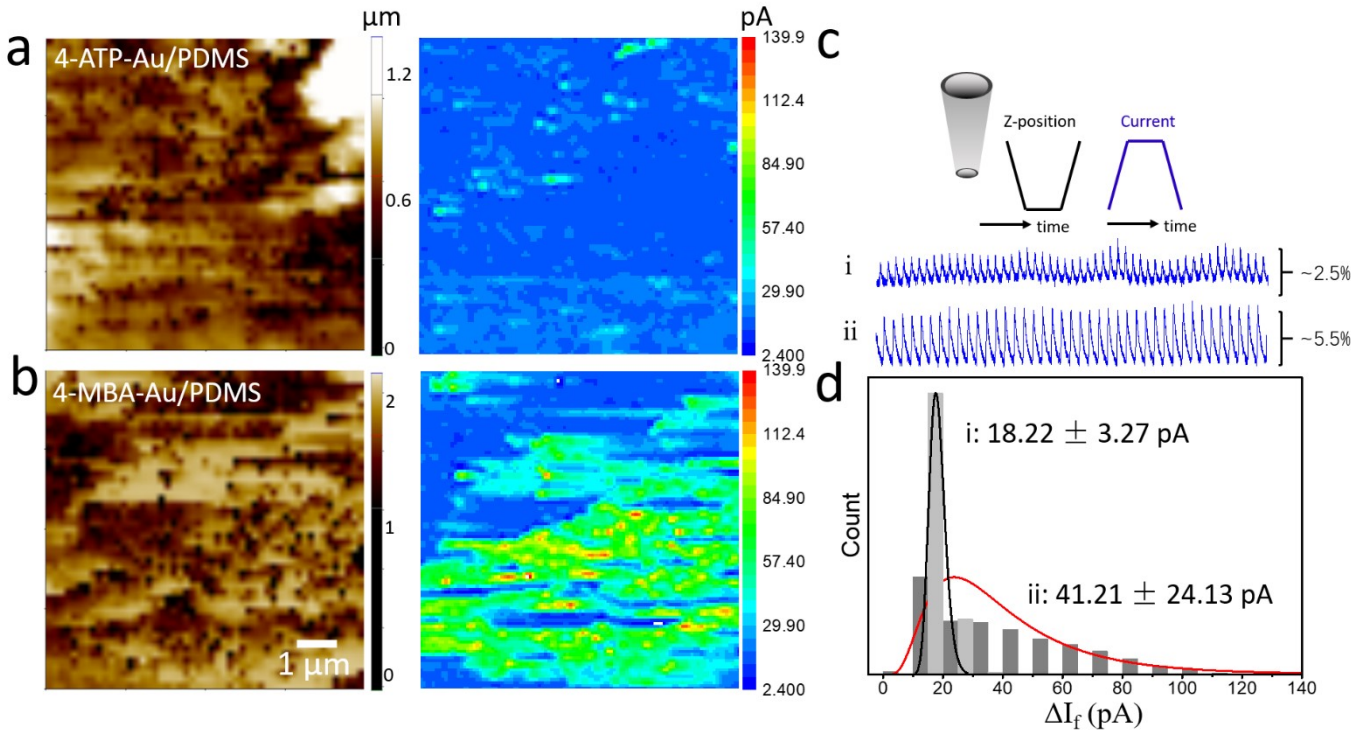

Figure S13. (a-b) The representative topography (left) and surface charge (ΔI_f) contrast images (right) of Au/PDMS substrates modified with 4-ATP **(a, positively charged)** and 4-MBA **(b, negatively charged)** using -0.1 V V_t. **(c-d)** The typical I_f time traces **(c)** and the ΔI_f histograms **(d)** on 4-ATP-Au/PDMS (i) and 4-MBA-Au/PDMS (ii) substrates.

ESI-8. Transmembrane potential measurements

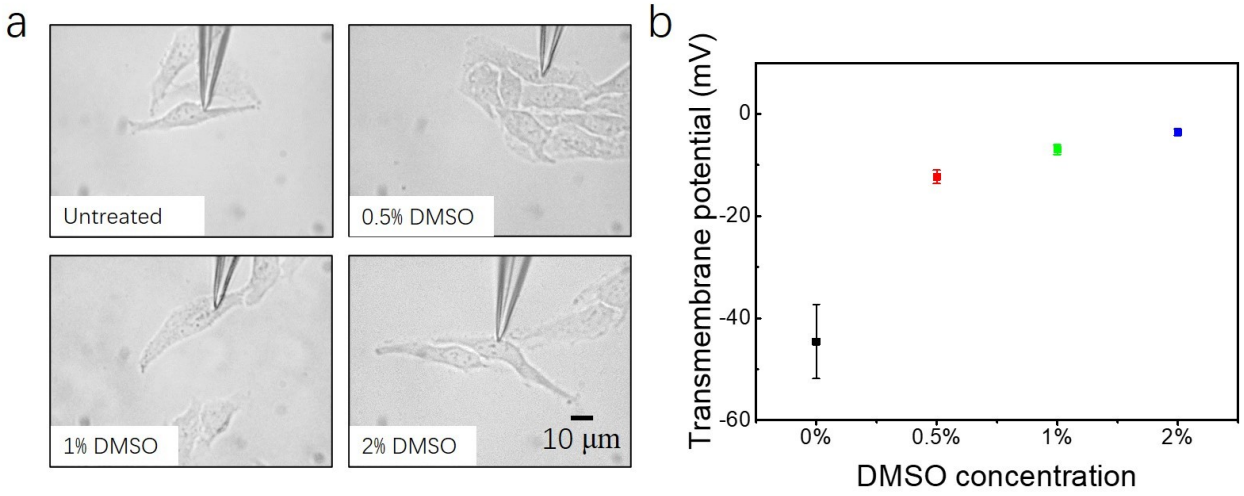

Figure S14. (a) Bright field microscope images of HeLa cells shortly after 30 min DMSO treatment with different concentrations. **(b)** Transmembrane potential of the HeLa cells after the treatment of DMSO. The average transmembrane potentials are untreated (-44.6±7.3 mV), DMSO [0.5%] (-12.3±1.3 mV), DMSO [1%] (-6.9±0.9 mV), and DMSO [2%] (-3.5±0.6 mV).

References

1. Panday, N.; Qian, G.; Wang, X.; Chang, S.; Pandey, P.; He, J., Simultaneous Ionic Current and Potential Detection of Nanoparticles by a Multifunctional Nanopipette. *ACS nano* 2016, 10, 11237-11248.
2. Chen, F.; Panday, N.; Li, X.; Ma, T.; Guo, J.; Wang, X.; Kos, L.; Hu, K.; Gu, N.; He, J., Simultaneous mapping of nanoscale topography and surface potential of charged surfaces by scanning ion conductance microscopy. *Nanoscale* 2020, 12, 20737-20748.
3. Bai, H. J.; Shao, M. L.; Gou, H. L.; Xu, J. J.; Chen, H. Y., Patterned Au/poly(dimethylsiloxane) substrate fabricated by chemical plating coupled with electrochemical etching for cell patterning. *Langmuir* 2009, 25, 10402-7.
4. Zhang, Q.; Xu, J. J.; Liu, Y.; Chen, H. Y., In-situ synthesis of poly(dimethylsiloxane)-gold nanoparticles composite films and its application in microfluidic systems. *Lab Chip* 2008, 8, 352-7.